NASA TECHNICAL MEMORANDUM

NASA TM X-52142

NASA TM X-52142

RESULTS OF HYPERVELOCITY IMPACTS INTO SPACE RADIATOR MATERIALS

by Nestor Clough, James H. Diedrich and Seymour Lieblein
Lewis Research Center
Cleveland, Ohio

TECHNICAL PREPRINT prepared for First Rankine Cycle Space Power Systems Specialists Conference sponsored by the American Institute of Aeronautics and Astronautics
Cleveland, Ohio, October 26-28, 1965

NATIONAL AERONAUTICS AND SPACE ADMINISTRATION · WASHINGTON, D.C. · 1965

RESULTS OF HYPERVELOCITY IMPACTS INTO SPACE RADIATOR MATERIALS

by Nestor Clough, James H. Diedrich and Seymour Lieblein

Lewis Research Center
Cleveland, Ohio

TECHNICAL PREPRINT prepared for

First Rankine Cycle Space Power Systems Specialists Conference
sponsored by the American Institute of Aeronautics and Astronautics
Cleveland, Ohio, October 26-28, 1965

NATIONAL AERONAUTICS AND SPACE ADMINISTRATION

RESULTS OF HYPERVELOCITY IMPACTS INTO SPACE RADIATOR MATERIALS

by Nestor Clough, James H. Diedrich and Seymour Lieblein

Lewis Research Center
National Aeronautics and Space Administration
Cleveland, Ohio

ABSTRACT

The results of an experimental hypervelocity impact program designed to evaluate various materials as armor for waste-heat radiator applications are discussed. Total damage, such as dimple, spall, and perforation, as well as simple cratering, was investigated in both flat plate and tubular targets. The experimental program was conducted on the ballistics range facilities of the General Motors Defense Research Laboratories under NASA contract. Projectiles of approximately 0.016 and 0.040 gram were accelerated to velocities of nominally 25,000 feet per second and impacted against various materials and configurations at room and elevated temperatures. The materials investigated include various aluminum alloys, stainless steel, columbium 1-percent zirconium, molybdenum, vanadium, tantalum, Inconel, A-286, L-605, graphite, and various types of beryllium. Significant differences in the ability of the various materials to resist dimple, spall, and perforation were observed in both flat plate and tubular configurations. The unique behavior of materials subjected to high-velocity impacts is clearly demonstrated.

Author

INTRODUCTION

The existence of a hazard to space vehicle components from the impact of meteoroids has been recognized as an important factor in the design of such components. In particular, space radiators contain fluid circuits that will have to be protected against critical damage from meteoroid impact. On a space radiator the thickness of the armor required to protect against critical damage by meteoroid impacts is determined by the vulnerable surface area, the time of exposure to the meteoroid hazard, and the damage characteristics of the armor material (ref. 1). Consequently, the radiator weight for a given application can vary widely depending on the severity of the meteoroid hazard and the material used for the armor. Recent information on the meteoroid hazard is given in references 2 and 3, and an example of the effects of different armor materials on radiator weight is given in reference 4.

The general cratering damage associated with hypervelocity impact into various materials is generally known (e.g., refs. 5 to 7). However, little information exists describing the specific damage likely to be incurred by the vulnerable components of space vehicles under operational conditions. The early published work on hypervelocity impact tests in various metals correlates the resulting crater depths with the target density and a strength property such as the modulus of elasticity or hardness (refs. 6 and 8). Examples of radiator analyses using a correlation based on material modulus of elasticity to predict the meteoroid crater depths in the armor are given in references 4, 9, and 10. In these analyses and in general radiator practice, and additional amount

of armor thickness is added to the crater depth to prevent perforation or critical damage of the armor wall. Because of a lack of detail data, all the armor materials are assumed to have the same material correlating coefficients and damage adjustments.

Recent results given in references 11 and 12 characterize the various types of damage that exist in tubes subjected to high velocity impacts. In addition to complete perforation, the inner surface of a tube could be made to dimple and spall with armor thicknesses significantly greater than the crater depth. The results of references 11 and 12 also indicate that the material coefficient for correlating simple penetration was unique to a particular material, and, therefore, it was assumed that the individual thicknesses to prevent dimple, spall, and perforation might also be peculiar to the material tested.

In order to assess the effects of individual material properties on the various correlating coefficients and critical damage in materials used in radiator weight calculations, the hypervelocity-impact-damage characteristics of 14 armor materials were investigated over a range of anticipated radiator-operating temperatures. The materials tested included several aluminum alloys, stainless steel, columbium 1-percent zirconium, molybdenum, vanadium, tantalum, Inconel, A-286, L-605, graphite, and several types of beryllium. The targets tested were in the forms of thick and thin flat plates, unlined tubes, and tubes with stainless steel liners.

The impact testing was performed on a ballistics range facility at the General Motors Defense Research Laboratories at Santa Barbara, Calif., as part of an overall research program on meteoroid protection concepts and

design data (NASA Contract Nos. NASw-468 and NAS3-2798). All impacts were carried out at a nominal velocity of 25,000 feet per second with either a 3/32 inch or a 1/8 inch diameter spherical pyrex projectile. In some cases 1/8 inch diameter spherical aluminum projectiles were used. A tabulation of the target configurations tested and conditions of impact is given in table I.

PLATE TARGETS

The impact data obtained from flat plate targets have been useful in determining damage information for use in radiator armor calculations (ref. 11). In plate targets, problems concerned with target fabrication are held to a minimum, and a relatively large target area can be used to ensure a reliable impact. Results concerning cratering materials coefficient and inner-surface damage obtained from impacts into flat plates will now be discussed.

MATERIALS COEFFICIENT

The estimation of the depth of penetration in a thick (semi-infinite) target due to spherical impacting particles has been made with various empirical equations. One such equation in which the penetration depth is correlated with the target-material modulus of elasticity and density is given from reference 8 as

$$\frac{P_\infty}{d} = \gamma\left(\frac{\rho_p}{\rho_t}\right)^{\varphi} \frac{(V)^{2/3}}{\left(\frac{E_t g}{\rho_t}\right)^{1/3}}$$

where

P_∞ penetration depth, in.

d projectile diameter, in.

γ materials coefficient

ρ_p projectile density, lb/ft^3

ρ_t target density, lb/ft^3

E_t Young's modulus, lb/ft^2

V projectile velocity, ft/sec

g 32.2, ft/sec^2

φ 1/2 or 2/3

Values of the materials coefficient γ have been reported to vary from around 1.5 to 2.5. In reference 1, an average value of 2.0 for $\varphi = 1/2$ was proposed for use if no explicit value corresponding to the target material in question was available. A value of 2.28 was proposed in reference 8 as obtained from lead and copper targets for $\varphi = 2/3$.

The various materials listed in table I were tested with the aim of defining the materials coefficient for each material and impact condition. In general, the materials were impacted in the form of thick flat plates at both room and elevated temperatures as given in table II. Equation (1) was solved for γ by using the measured values of P_∞ obtained from the tests and the values of Young's modulus as given in the table. Table II also includes a description of the targets impacted, impacting projectile mass and velocity, measured penetration depth P_∞, and the various materials specific gravities used in the calculations for γ. The individual calculated values of γ presented are for a value of $\varphi = 1/2$.

The average values of γ for the various materials and impact temperatures are summarized in table III. The values of γ are seen to vary considerably from a low of 1.13 for ATJ graphite to a high of 2.58 for 356-T51 cast aluminum. The variation of the values of γ calculated for room temperature impacts indicates the uniqueness of the materials coefficient for a particular armor material. Furthermore, the values of γ for each material are not constant with temperature. The value of γ for the refractory materials are seen to generally increase with temperature, whereas the other materials show

a slight decrease or no change with temperature. This variation of γ with temperature needs further amplification, however, since some of the values in table III are based on single impacts. These experimental values of γ for use in equation (1) can now form the basis for further design calculations and comparisons involving specific armor materials.

Inner Surface Damage

The major interest to the designer of a space radiator is the damage caused by an impacting particle to the internal flow passage rather than the depth of penetration of the armor. In reference 11, it was established that damage modes other than complete perforation of the radiator tube exist, which may be critical to the successful operation of the radiator. In particular, the inner surface of a tube could be made to deform and spall with armor thicknesses signficantly greater than the crater depth. Therefore, it was necessary to study the effects of pertinent variables on inner-surface damage for a wider range of materials.

Test conditions.- The targets utilized in this series of tests consisted of flat plates of 2024-T6 aluminum, 316 stainless steel, columbium 1-percent zirconium, A-286, L-605, and Inconel 718. The experimental procedure involved impacting flat plate targets at room temperature with progressively less thicknesses until complete perforation of the targets was observed. The targets were then sectioned at the point of maximum crater depth and examined. Generally, each target configuration required 5 to 8 impacts to define the thicknesses at which the various modes of rear surface damage occurred.

The definition of the damage modes of interest, as they will be used herein, is shown in figure 1. Dimple is defined as any measurable permanent displacement of the surface below the crater without dislodgement of material, spall is a breaking away of any part of the surface of the target below the crater, and perforation is used in the conventional sense. In these tests,

the objective was to define the points of incipient rear-surface-damage Visual observations of the sectioned targets was utilized to qualitatively classify the degree of damage and to establish the incipient conditions.

A tabulation of all the shots fired in conjunction with this phase of the program is given in table IV. The table includes a complete description of the targets impacted (i.e., material, armor thickness, dimensions), the conditions of impact (i.e., projectile mass and velocity), and a qualitative description of the rear surface damage sustained by the targets. Representative sectioned targets after impact are shown in Figure 2 for the columbium-alloy targets tested. The figure clearly depicts the transition from simple penetration to perforation with varying degrees of spall between. It is clear from the photograph that the damage incurred in a high-velocity impact of a thin section can be greatly extended beyond that of simple crater formation.

Damage thickness factors.- From examination of the sectioned targets impacted in this phase of the program, it was possible to closely estimate the target thickness corresponding to the onset of perforation, spall, and dimple. For each material, damage-thickness factors were defined for each damage mode as the value of the target thickness at threshold damage (i.e., either dimple, spall, or perforation) t^*, divided by the semi-infinite penetration depth P_∞, as obtained from equation (1).

Damage thickness factors t^*/P_∞ were determined for six materials and the results are summarized in table V. The factors are seen to vary considerably for all three modes of damage among the materials tested. The results show that the damage thickness factor at perforation is not a constant value for all the materials, as has been previously assumed. (A value of $t^*/P_\infty = 1.5$ to prevent perforation has been widely used). Furthermore,

although the columbium alloy tested has a damage thickness factor at perforation consistent with the other high strength alloys tested, the values of t^*/P_∞ for the columbium at spall and dimple thresholds are from 1.5 to approximately twice the corresponding damage factor values for the other materials tested.

It should be noted that the damage factors given in table V define incipient damage conditions and therefore will not be adequate to completely prevent the particular mode of damage. An increase in the design thickness above the values indicated by these factors will generally be necessary to prevent occurrence of the chosen damage.

TUBULAR TARGETS

Prior results reported in reference 11 indicated that the damage thickness factors determined using flat plates may not be identical to those in comparable tubular configurations. Consequently, tests of comparable impacts on lined and unlined tubes were conducted.

Unlined Tubes

In this study using unlined tubular targets of 316 stainless steel and 2024-T6 aluminum, the effects of the magnitude of tube inside diameter on inner surface dimple, spall, and perforation were investigated. The results are presented in table VI, which contains the shot identification, target dimensions and materials, conditions of impact (i.e., projectile mass, velocity, impact angle), a description of the inner surface damage, and the various calculations used later in determining the damage thickness factors. Representative sectioned targets after impact are shown in figure 3 which illustrates the three damage modes.

The threshold damage thickness factors for the tubular targets tested were determined in the same fashion as for the aforementioned flat plate targets. For this case, however, the normal component of the impact velocity was used in equation (1) for the calculation of P_∞. This procedure was shown to be valid in reference 11. Factors for incipient dimple, spall, and perforation were plotted against the inverse of the tube inside diameter as shown in figure 4. The variations given in figure 4 were determined visually from the sectioned targets and represent a best estimate of the points of incipient conditions. The damage thickness factors for the flat plates (1/I.D = 0) were obtained from the thin plate study discussed previously.

Figure 4 indicates that a slight reduction in required armor thickness at perforation, spall, or dimpling can be obtained with reduced tube inside diameter. The variations indicate that the tube-size effect is very small for 316 stainless steel tubes in all three modes of damage. For the aluminum alloy tested, the general trend of reduced damage thickness factors with reduced tube inside diameter is also apparent. It appears that the largest variation of t^*/P_∞ with tube inside diameter is for the onset of spall in the aluminum tested. The trend of reduced damage factors with reduced tube inside diameters may be associated with the increased ability of a curved surface to tolerate a given shock loading without fracture. The curved inner surface of a tube under the point of impact has to go through a compressive loading condition as it is deformed before it can be stressed in tension. Therefore, if the free surface tensile strength is important in suppressing damage, reduced inside diameter tubes will have effectively higher free surface tensile strengths and will tend to supress inner surface damage.

The observed variations of damage factors with tube radius indicate that, for more exact design information, the damage factors should be determined with the configuration and material in question. However, the tests

indicate that in all cases the flat plate values of the damage thickness factors are slightly conservative compared with the tube values and, therefore, can be applicable to general design usage.

Lined Tubes

Preliminary results of impacts into cast 356-T51 aluminum over L-605 liners, reported in reference 11, indicated that the liner could deform drastically without rupture or spall for the particular target-material combinations tested. A series of experiments was performed in order to further explore the characteristics of lined tubes and to quantitatively assess the advantages of lined tubes compared with unlined tubes. These experiments used 356-T51 cast aluminum armor over 316 stainless steel liners of various thicknesses and inside diameters as listed in table VII. As before, the aluminum armor thickness was successively reduced to define the threshold thickness for the three significant damage modes. In these tests, however, the critical damage was the damage that occurred on the inner surface of the liner.

For the liner-armor combinations impacted in this series of tests, it was found that for the 0.015 and 0.028 inch liner thicknesses the transition from liner dimpling to liner perforation was completed with no evidence of liner spall, and, in some cases, complete closure of the tube by the liner was observed without puncture of the liner. However, for the tubes with liner thickness of 0.065 inch spall occurred on the inner surface of the liner. Figure 5 illustrates these effects for the three liner thicknesses with 0.5 inch inside diameter tubes. These results indicate that the liner, although it acts to effectively suppress armor spall, can, in some cases, spall itself under the correct conditions of impact and thickness.

In order to investigate the possible existence of an optimum value of liner thickness to prevent perforation damage without spall, a series of tests was performed on tubes with 0.5 inch inside diameters and liners with thicknesses of 0 (no liner), 0.015, 0.028, and 0.065 inch. As before, the armor thickness was varied to define the required total thickness (armor and liner) to prevent perforation. From these results it was possible to deduce an incipient perforation line as a function of liner thickness by plotting the total effective weight of armor and liner (per inch of length) for the particular observed damage modes against effective liner thickness.

The effective thicknesses (armor and liner) from which the effective weights were determined, represent values normalized to standard impact conditions at 25,000 feet per second. These effective thicknesses were determined from the relation

$$t_{eff} = t_a \left(\frac{P_{\infty\ eff}}{P_{\infty\ a}} \right) \tag{2}$$

where the subscripts eff and a refer to effective and actual, respectively. By using equation (1) for P_∞,

$$t_{eff} = t_a \left(\frac{V_{eff}}{V_a} \right)^{2/3} \tag{3}$$

where V_{eff} is set equal to 25,000 feet per second.

Figure 6 shows the results of this series of tests in the form of a plot of effective tube weight against effective liner thickness for the conditions of dimple, spall, and perforation, The minimum value of tube specific weight, as obtained from the faired curve, indicates the existence of an optimum liner thickness between 0.025 and 0.050 inch for incipient perforation of the liner without spall for these particular conditions if impact. Previous tests had shown that at failure the tube

would close completely without rupturing the inner liner. This immediately raised the possibility of allowing a wide "degree" of dimple or closure damage not possible in unlined tubes. Thus, if a partial or nearly full closure of the fluid carrying passage without rupturing of the inner liner can be accepted in the design, a sizable weight saving may be possible.

A series of tests was run in which tubes with optimum liners (0.028-in. thick) were impacted with varying thicknesses of armor. The armor thickness was varied so that the complete range of internal damage was observed (i.e., complete closure to no dimple). The results of the tests are shown graphically in figure 7, where the damage thickness factor for the aluminum armor t^*/P_∞ is plotted against the ratio of dimple height to tube inside diameter. The damage factors are seen to vary from 0.9 for complete closure to 2.5 for no dimple. It appears that for these lined tubes a substantial armor weight saving is possible if a degree of damage is allowed beyond no dimple. For example, an allowable dimple height of only 25 percent of the tube inside diameter results in reducing the thickness of armor required to suppress dimple damage by 50 percent.

It should be remembered however, that these factors and discussions refer only to the particular liner-armor combinations tested and the particular energy level of impacts employed in these tests. The nature of the liner-armor bond may have an important effect in the type of inner-surface damage observed. As yet, the relative importance of a physical interface as compared with an integral bond between the liner and armor (impedance mismatch) is unexplored under the conditions of hypervelocity impact. The cast aluminum over steel liner targets used in these tests had physical interfaces rather than integral bonds. Caution must therefore be used when these results are extended to other liner-armor combinations.

BERYLLIUM IMPACTS

The targets tested in this series of experiments consisted of tubular beryllium armor 1.25-inch outside diameter and a 0.375-inch wall thickness surrounding a 0.50-inch outside diameter liner tube of AISI-316 stainless steel or columbium - 1-percent zirconium. The liner thicknesses were 0.028 and 0.050 inch for the stainless steel and columbium alloy, respectively. The 0.375-inch beryllium armor thickness was selected to prevent perforation of the liner tube but to permit internal dimpling.

The tubular beryllium armor was bonded to the liner tube by three different methods: (1) by placing solid extruded beryllium tubing around the liner tube, (2) by cold-pressing beryllium powder around the liner tube and sintering by the simultaneous application of heat and pressure, or (3) by casting beryllium directly around the liner tube. Specific details of these fabrication processes together with the chemical composition of the beryllium armor are found in references 13 and 14.

Figure 8 illustrates the external impact damage on targets fabricated by the different processing methods. All the targets shown on the figure were impacted at a nominal temperature of 1300° F. The hemispherical crater surrounded by a spalled region is characteristic of impact damage encountered in beryllium targets (ref. 12). As shown on the figure, the beryllium armor remained intact around the liner tube even though extensive cracking damage occurred.

The damage to the inner surface of the liner tubes for all the targets shown on figure 8 was confined to a dimple inside the tube bore. Little difference in the pattern of observed damage shown on figure 8 resulted when beryllium targets were tested at room temperature (ref. 12). In reference 12, one beryllium tube target was also impacted by two equal-energy

impacts in the same plane approximately 120° apart. No large armor fragments were dislodged by the impacts, and only a connecting fracture was observed between the two impact points. The average materials coefficient obtained for the beryllium impact tests in reference 12 was 2.28.

The cracking damage encountered on the beryllium targets prompted the fabrication of tubular beryllium targets reinforced with small randomly oriented stainless steel fibers or with two concentric cylinders of wire mesh. The details pertaining to the fabrication of the reinforced targets are presented in reference 15. Impact tests conducted on the reinforced targets did not reveal any major tendencies toward reduction of the external damage as shown in figure 9. The figure shows that the general features and severity of the external damage were similar to those encountered on targets without reinforcements.

In order to gather more complete information on the effect of the internal reinforcements, the steel-mesh and steel-fiber reinforced beryllium targets and the impact target armored only with sintered powder were cut and polished for examination. These polished cross sections are shown in figure 10. The internal-damage features are approximately the same for all targets shown. The reinforced configurations, however, had less cracking damage adjacent to the liner tube under the impact point. None of the cross sections had any observable bond remaining between the armor and liner after impact, and several localized bond failures are evident in several beryllium steel-reinforcement interfaces. Radial cracks are also visible diametrically opposite the impact point in the rear portions of the sintered powder armor and the fiber-reinforced armor.

These limited observations indicate that some potential benefits can be gained by reinforcing beryllium armor; however, sounder, more integral

bonds are required. Also, the extensive, internal-cracking damage in the beryllium armor can severely reduce the structural capability of the armor, depending on the particular design application.

RADIATOR WEIGHT COMPARISONS

The experimentally obtained values of damage factors for dimple, spall, and perforation for the specific materials investigated can now permit a more definite comparison of the specific weights of radiators with these materials as meteoroid armor. Computations similar to those in reference 4 were made for a flat-plate, direct-condensing radiator with a central fin-tube cross section by using the procedures and computer program described in reference 9. The particular cycle conditions chosen for the comparison were 300-kW-output Rankine cycle system, turbine inlet temperature of 1850° F, potassium working fluid, mission time of 500 days, probability of no meteoroid critical damage equal to 0.95, and a surface emittance of 0.90. The materials included in the comparison were columbium - 1-percent zirconium, Inconel 718, L-605, 316 stainless steel, TZM molybdenum, vanadium, ATJ graphite, and beryllium. The graphite- and beryllium-armored radiators included an inner liner tube of columbium - 1-percent zirconium. The balance of the materials were used without internal liners.

A comparison of the calculated radiator weights for the design condition of no allowable spall, because of potential damage to rotating components, is shown in figure 11. The damage thickness factors used for each material to prevent inner-surface spall were taken as the experimentally determined factors at incipient dimpling. For the lined tubes, the damage factor used corresponded to an allowable liner dimple height of around 25 to 30 percent of the diameter. The results of the calculations shown on figure 11 indicate that beryllium and graphite continue to maintain their potential low-specific-

weight advantage for armor. A graphite-armored radiator is potentially now only 20 percent heavier than a beryllium armored radiator (because of the low value of γ for graphite). These results, however, are based on equal values of liner-damage factors, which have not yet been verified. Also, the radiator-vehicle support structure is not included. The poor showing of the columbium - 1-percent-zirconium alloy, results from its large value of spall damage factor.

A considerable reduction in radiator weight can be obtained with monometallic radiator tubes if the prevention of perforation rather than the prevention of spall can be adopted as the critical design criterion. Such a situation is possible with an all-liquid coolant radiator in conjunction with a heat exchanger vapor condenser and a nonrotating (e.g., electromagnetic) circulating pump. An indication of the calculated weight saving when designing to prevent perforation with stainless steel and columbium - 1-percent zirconium is shown in figure 12.

The results of figures 11 and 12 vividly indicate the individual behavior of each armor material and accent the need for further detailed impact-test data for specific radiator materials, constructions, and applications.

CONCLUSIONS

The following are the major results of the hypervelocity impact tests conducted on space radiator materials:

(1) Each of the materials tested had a unique cratering behavior as evidenced by the wide range of values obtained for the materials coefficient γ used in the correlating expression for crater depth. The required armor thickness defining the onset of dimple, spall, or perforation damage was also found to vary with the target material for flat-plate targets tested

at room temperature. Tubular targets of 316 stainless steel and 2024-T6 aluminum each displayed a slight tendency toward reduced dimple and spall damage thickness factors as tube inside diameter decreased.

(2) For tubes with thin-walled liners, only dimple and perforation remained as active damage modes. For cast 356-T51 aluminum armor over 316 stainless steel liners, the liner wall thickness for minimum total weight to prevent liner perforation ranged from 0.025 to 0.050 inch. Sizable reductions in armor weight are possible if increased dimple heights are allowed in the internal tube liner. For beryllium tubes, the use of steel fibers or mesh reinforcements imbedded in the beryllium armor tend to reduce cracking damage only slightly.

(3) Calculated radiator specific weights with the experimental-materials constants and damage-thickness factors resulted in wide variations in radiator weight depending on the damage mode and the armor material used. There is a need for further impact data on specific-armor materials and radiator constructions as applied to specific power systems.

REFERENCES

1. Loeffler, I. J., Lieblein, S., and Clough, N.: Meteoroid Protection for Space Radiators. Progress in Astronautics and Aeronautics, Vol. 11 Power Systems for Space Flight, Academic Press, New York, N. Y., p. 551-579, 1963.
2. Loeffler, I. J., Clough, N., and Lieblein, S.: Recent Developments in Space Power Systems Meteoroid Protection. Paper presented at Aerospace Power Systems Conf., AIAA, SAE, ASME, IAPE, Electron Div. Group IEEE, Phila. (Penn)., Sept. 1, 1964.
3. Clough, N., and Lieblein, S.: Significance of Photographic Meteor Data in the Design of Meteoroid Protection for Large Space Vehicles. NASA TN D-2958, 1965.
4. Diedrich, J. H., and Lieblein, S.: Materials Problems Associated with the Design of Radiators for Space Powerplants. Progress in Astronautics and Aeronautics, Vol. 11 - Power Systems for Space Flight, Academic Press, New York, N. Y., p. 627-653, 1963.
5. Bjork, R. L.: Meteoroids vs. Space Vehicles. ARS Journal, Vol. 31, No. 6, June 1961, p. 803-807.
6. Eichelberger, R. J., and Gehring, J. W.: Effects of Meteoroid Impacts in Space Vehicles. ARS Journal, Vol. 32, No. 10, Oct. 1962, p. 1583-1591.
7. Summers, J. L., and Charters, A. C.: High-Speed Impact of Metal Projectiles in Targets of Various Materials, Vol. I of Proc. of the Third Hypervelocity Impact Symposium, Armour Res. Foundation, Feb. 1959, p. 101-113.
8. Summers, J. L.L Investigation of High-Speed Impact: Regions of Impact and Impact at Oblique Angles. NASA TN D-94, 1959.

9. Krebs, R. P., Haller, H. C., and Auer, B. M.: Analysis and Design Procedures for a Flat, Direct-Condensing, Central Finned-Tube Radiator. NASA TN D-2474, September, 1964.

10. Saule, A. V., Krebs, R. P., and Auer, B. M.: Design Analysis and General Characteristics of Flat-Plate Central-Fin-Tube Sensible-Heat Space Radiators. NASA TN D-2839, June 1965.

11. Lieblein, S., Clough, N., and McMillan, A. R.: Hypervelocity Impact Damage Characteristics in Armored Space Radiator Tubes. NASA TN D-2472, 1964.

12. Diedrich, J. H., Loeffler, I. J., and McMillan, A. R.: Hypervelocity Impact Damage Characteristics in Beryllium and Graphite Plates and Tubes. NASA TN D-3018, 1965.

13. Diersing, R. J., Hanes, H. D., and Hodge, E. S.: Fabrication of Beryllium-Clad Tubular Hypervelocity Impact Targets by Gas Pressure Bonding. NASA CR-54058, 1963.

14. Patenaude, C. J., and Santschi, W. H.: Casting of Beryllium - Stainless Steel and Beryllium - Columbium Impact Target Composites. NASA CR-54144, 1964.

15. Diersing, R. J., Carmichael, D. C., Hanes, H. D., and Hodge, E. S.: Gas-Pressure Bonding of Stainless Steel-Reinforced Beryllium Hypervelocity Impact Targets. NASA CR-54222, 1964.

TABLE I. - DESCRIPTION OF TARGETS TESTED

Target material	Configuration			Test temperature, °F				
	Tube		Flat plate					
	Lined	Unlined		Room	400°	700°	1300°	2000°
Aluminum (7075-T6)			x	x		x		
(356-T51)	x		x	x		x		
(2024-T6)		x	x	x	x	x		
Cobalt (L-605)			x	x				
Columbium (Cb-1Zr)			x	x		x	x	x
Molybdenum (TZM)			x	x				x
Nickel (Inconel 718)			x	x				
Stainless steel (316)		x	x	x		x	x	
Steel (A286)			x	x				
Tantalum			x	x			x	x
Vanadium			x	x			x	x

TABLE II. - THICK PLATE TEST RESULTS

Target material	Specific gravity	Impact, round number	Projectile[a]				Target			Calculated Materials coefficient γ
			Diameter, d, in.	Material	Mass, g	Impact velocity V, ft/sec	Temperature, ^{o}F	Crater depth P_{∞}, in.	Modulus of elasticity E_t, lb/ft^2	
Aluminum (7075-T6)	2.80	221	1/8	Pyrex	0.0409	25,900	Room	0.311	15.00×10^8	1.93
		223	1/8	Pyrex	.0411	25,700	700	.362	5.76	1.68
		239	1/8	Aluminum	.0414	26,900	Room	.316	15.00	1.92
Aluminum (356-T51	2.68	355	3/32	Pyrex	0.0178	24,600	700	0.302	9.08×10^8	2.21
		99	1/8	Pyrex	.0418	20,300	Room	.305	15.00	2.26
		127	1/8	Pyrex	.0413	25,800	Room	.466	15.00	2.92
		128	1/8	Pyrex	.0413	24,700	Room	.396	15.00	2.57
		164	1/8	Pyrex	.0413	22,100	700	.403	9.08	2.38
		176	1/8	Pyrex	.0416	24,200	700	.405	9.08	2.33
Aluminum (2024-T6)	2.77	446	1/8	Pyrex	0.0412	24,800	Room	0.321	15.00×10^8	1.97
		449	1/8	Pyrex	.0412	25,000	700	.375	9.08	2.06
		454	1/8	Pyrex	.0414	25,000	400	.366	12.95	2.25
Columbium-1 percent zirconium	8.66	94	1/8	Pyrex	0.0416	23,700	Room	0.156	23.10×10^8	1.46
		95	1/8	Pyrex	.0431	20,400	Room	.136	23.10	1.41
		97	1/8	Pyrex	.0416	24,000	Room	.158	23.10	1.46
		101	1/8	Pyrex	.0422	16,000	Room	.097	23.10	1.18
		102	1/8	Pyrex	.0419	20,200	Room	.131	23.10	1.37
		103	1/8	Pyrex	.0417	24,200	Room	.157	23.10	1.45
		320	3/32	Pyrex	.0176	24,800	700	.140	22.30	1.67
		353	1/8	Pyrex	.0416	25,000	1300	.207	20.90	1.83
		544	1/8	Pyrex	.0409	25,300	2000	.220	15.85	1.76
Stainless steel (316)	8.01	337	1/8	Pyrex	0.0429	24,200	Room	0.152	40.60×10^8	1.68
		403	1/8	Pyrex	.0422	25,300	Room	.160	40.60	1.71
		338	1/8	Pyrex	.0412	24,700	700	.177	37.40	1.87
		339	1/8	Pyrex	.0412	24,700	1300	.199	30.30	1.95
		350	1/8	Aluminum	.0468	25,300	Room	.156	40.60	1.62
Molybdenum (TZM)	10.2	340	1/8	Pyrex	0.0412	25,400	Room	0.120	66.30×10^8	1.57
		547	1/8	Pyrex	.0421	25,000	2000	.175	49.70	2.09

TABLE II. CONCLUDED

Target material	Specific gravity	Impact, round number	Projectile[a]				Target			Calculated Materials coefficient γ
			Diameter, d, in.	Material	Mass, g	Impact velocity V, ft/sec	Temperature, ^{o}F	Crater depth P_{∞} in.	Modulus of elasticity E_t, lb/ft^2	
Tantalum	16.6	384	1/8	Pyrex	0.0410	25,700	Room	0.121	39.90×10^8	1.42
		385	1/8	Pyrex	.0411	25,200	1300	.142	35.30	1.65
		543	1/8	Pyrex	.0411	25,000	2000	.152	32.40	1.71
Vanadium	6.11	386	1/8	Pyrex	0.0414	25,200	Room	0.154	27.40×10^8	1.38
		389	1/8	Pyrex	.0411	25,600	1300	.194	25.40	1.68
		548	1/8	Pyrex	.0422	24,350	2000	.231	18.70	1.80
Steel (A-286)	7.92	1257	3/32	Pyrex	0.0183	25,000	Room	0.129	41.60×10^8	1.99
Cobalt (L-605)	9.13	1253	3/32	Pyrex	0.0178	23,500	Room	0.109	46.80×10^8	1.77
Nickel (Inconel 718)	8.21	1256	3/32	Pyrex	0.0178	24,900	Room	0.103	41.70×10^8	1.55

[a]Average calculated specific gravity; 2.50 for 3/32-inch-diameter Pyrex sphere, 2.48 for 1/8-inch-diameter Pyrex sphere, and 2.63 for 1/8-inch-diameter aluminum sphere.

TABLE III. - SUMMARY OF AVERAGE MATERIALS COEFFICIENTS γ

Target material (alloy)	Target temperature, °F				
	Room	400°	700°	1300°	2000°
Aluminum (7075-T6)	1.93		1.68		
(356-T51)	2.58		2.31		
(2024-T6)	1.97	2.25	2.06		
Columbium (1 percent Zr)	1.39		1.67	1.83	1.76
Steel (316)	1.67		1.87	1.95	
(A286)	1.99				
Molybdenum (TZM)	1.57				2.09
Tantalum	1.42			1.65	1.71
Vanadium	1.38			1.68	1.80
Beryllium[a]	2.05		2.38	2.30	
Graphite[a] (ATJ)	1.18			1.13	
Nickel (Inconel 718)	1.55				
Cobalt (L605)	1.77				

[a]Data from reference 10.

TABLE IV. - THIN PLATE DATA

Round	Target material	Target thickness, t, in.	Projectile mass, g	Projectile velocity V ft/sec	Penetration depth, in.	Semi-infinite penetration depth, P_∞, in.	Rear surface damage[a]	Ratio t/P_∞
519	Stainless steel (316)	0.179	0.0163	24,900		0.138	P	1.38
486		.200	.0156	25,200	0.144	.129	S	1.55
480		.224	.0159	24,900	.128	.129	S	1.74
483		.240	.0163	25,300	.130	.130	S	1.85
487		.300	.0156	25,200	.128	.129	D	2.32
488	Aluminum (2024-T6)	0.325	0.0160	24,800		0.203	P	1.65
489		.330	.0157	23,900		.197	P	1.68
514		.375	.0163	24,400	0.219	.201	S	1.87
482		.450	.0157	25,100	.206	.203	S	2.22
481		.470	.0156	24,800	.203	.200	D	2.35
963		.475	.0178	24,600	.190	.205	D	2.32
478		.483	.0157	24,000	.196	.197	D	2.45
1129	Columbium-1 percent zirconium	0.276	0.0421	23,500		0.163	P	1.69
1077		.300	.0415	25,000	0.228	.170	S	1.77
1076		.350	.0415	24,800	.167	.169	S	2.07
1130		.400	.0420	22,800	.160	.160	S	2.50
1131		.454	.0418	23,300	.171	.163	S	2.78
1194		.550	.0418	23,400	.164	.163	S	3.35
1195		.650	.0405	24,000	.159	.164	S	3.96
1196		.750	.0412	24,600	.150	.168	D	4.47
1292	Steel (A-286)	0.186	0.0172	25,000		0.126	P	1.48
1291		.203	.0173	24,400	0.129	.124	S	1.64
1261		.218	0.181	24,700	.128	.128	S	1.70
1257		.230	.0183	25,000	.129	.129	S	1.79
1266		.292	.0174	24,500	.115	.125	D	2.33
1251	Cobalt (L605)	0.182	0.0180	24,100		0.112	P	1.62
1250		.204	.0181	24,200	0.117	.112	S	1.82
1252		.232	.0176	24,300	.104	.112	S	2.07
1253		.254	.0178	23,500	.092	.109	D	2.33
1293		.273	.0177	24,900	.114	.114	D	2.39
1295	Nickel (Inconel 718)	0.193	0.0176	24,700	0.134	0.107	S	1.80
1294		.215	.0177	24,800	.110	.110	S	1.96
1254		.230	.0179	24,000	.109	.107	S	2.15
1255		.263	.0183	24,700	.109	.110	S	2.40
1256		.292	.0180	24,900	.103	.103	D	2.84
1296		.315	00177	24,800	.107	.107	D	2.94

[a]Perforation, spall, and dimple are designated by P, S, and D.

TABLE V. - DAMAGE-THICKNESS FACTORS t^*/P_∞ FOR FLAT PLATES

Target material	Damage mode		
	Dimple	Spall	Perforation
Aluminum (2024-T6)	2.5	2.3	1.7
Steel (316)	2.4	1.9	1.4
(A286)	~2.4	1.9	1.4
Columbium (1 percent zirconium)	4.5	4.0	1.7
Nickel (Inconel 718)	~3.0	2.5	
Cobalt (L605)	~2.5	2.1	1.7

TABLE VI. - UNLINED TUBE TEST RESULTS

Round	Target material	Tube inside diameter, in.	Target thickness, t, in.	Projectile mass, g	Projectile velocity, V, ft/sec	Impact angle, λ, deg	Calculated semi-infinite penetration depth P_∞, in.	Ratio t/P_∞	Inner surface damage[a]
599	316-S.S.	0.288	0.151	0.0174	24,400	20	0.125	1.21	P
598			.181	.0173	24,100	30	.117	1.55	S
580			.205	.0175	23,700	32	.115	1.78	D
552	316-S.S.	0.500	0.175	0.0173	24,800	27	0.122	1.44	S
531			.208	.0160	25,100	16	.126	1.65	S
530			.216	.0160	24,800	27	.119	1.82	S
479			.223	.0157	24,200	0	.123	1.78	S
517			.231	.0162	24,700	2	.127	1.82	S
532			.240	.0159	24,800	20	.123	1.95	B
491			.240	.0157	25,600	32	.111	2.16	D
553	316-S.S.	1.00	0.175	0.0172	24,550	14	0.128	1.37	P
560			.190	.0170	25,800	0	.134	1.42	S
525			.224	.0159	24,600	7	.127	1.76	S
559			.230	.0170	25,800	10	.133	1.73	S
551			.239	.0175	24,500	8	.129	1.85	B
550			.239	.0182	24,400	32	.119	2.01	D
558			.245	.0170	26,000	12	.133	1.84	S
614	2024-T6Al	0.250	0.300	0.0175	24,100	28	0.190	1.57	S
612			.300	.0175	23,400	20	.195	1.54	S
583			.325	.0175	24,000	30	.186	1.73	S
573			.361	.0172	25,200	9	.209	1.73	S
602			.375	.0170	23,700	42	.165	2.28	D
568			.482	.0172	24,600	27	.192	2.50	D
579	2024-T6Al	0.500	0.325	0.0174	24,400	5	0.205	1.59	P
572			.361	.0172	25,000	33	.186	1.94	S
601			.379	.0170	24,500	17	.199	1.90	B
595			.422	.0173	24,100	28	.192	2.19	D
567			.482	.0172	25,200	8	.209	2.30	D

TABLE VI. CONCLUDED

Round	Target material	Tube inside diameter, in.	Target thickness, t, in.	Projectile mass, g	Projectile velocity, V, ft/sec	Impact angle, λ, deg	Calculated semi-infinite penetration depth P_∞, in.	Ratio t/P_∞	Inner surface damage[a]
575	2024-T6Al	1.00	0.325	0.0172	25,100	9	0.209	1.56	P
571			.361	.0172	25,600	20	.204	1.72	S
570			.361	.0173	24,800	32	.172	2.10	S
600			.397	.0173	24,800	42	.187	2.12	D
594			.422	.0171	25,000	20	.200	2.11	D
560			.482	.0178	25,000	0	.209	2.30	D

[a]Perforation, spall, dimple, and broken bubble are designated by P, S, D, and B.

TABLE VII. - LINED TUBE TEST RESULTS FOR 356-T51 CAST ALUMINUM OVER 316 STAINLESS STEEL LINERS

Round	Liner inside diameter, in.	Liner thickness, t_L, in.	Armor thickness, t_a, in.	Projectile velocity, V, ft/sec	Impact angle, λ, deg	Effective liner thickness, t_L^*, in.	Effective armor thickness, t_a^*, in.	Effective target weight, lb/in.	Liner damage description[a]
720	0.320	0.028	0.188	24,000	15	0.0294	0.198	0.0359	D (Severe)
805	.320	.028	.162	25,200	20	.0290	.168	.0405	C
677	0.500	0.015	0.185	23,500	30	0.0172	0.212	0.0605	P
800	↓	.028	.122	25,100	30	.0302	.134	.0462	C
717		.028	.142	23,500	38	.0342	.174	.0606	D
670		.028	.172	23,100	23	.0312	.192	.0634	D
668		.065	.095	23,500	20	.0705	.103	.0627	P (Severe)
669		↓	.095	23,500	18	.0702	.103	.0623	P (Severe)
695			.125	24,000	28	.0723	.139	.0747	S
802	↓	↓	.135	24,900	10	.0660	.137	.0700	P
809	1.195	0.028	.174	24,500	15	0.0290	0.180	0.1196	P (Severe)
718	↓	↓	.192	24,000	14	.0294	.202	.1321	D
807			.224	23,500	15	.0298	.239	.1552	D
799			.250	24,900	7	.0282	.251	.1594	D
796	↓	↓	.274	25,200	0	.0279	.273	.1719	D
954	0.500	0.015	0.485	24,800	17.5	0.0156	0.503	0.1847	D
969	↓	.015	.360	24,000	10	.0156	.374	.1237	D
967		.028	.137	24,000	40	.0344	.168	.0599	D (Severe)
966		.028	.397	24,500	15	.0290	.411	.1418	D
970		.065	.215	24,000	40	.0796	.264	.1332	↓
971	↓	.065	.290	24,700	35	.0751	.335	.1374	
964	0.320	0.028	0.237	24,500	27.5	0.0307	0.260	0.0683	↓
968	.320	↓	.312	24,300	0	.0285	.317	.0856	
960	1.195	↓	0.379	24,500	7.5	0.0286	0.388	0.2540	↓
959	1.195		.500	24,800	30	.0309	.553	.3820	

[a]Dimple closure, perfection, and spall are designated by D, C, P, and S.

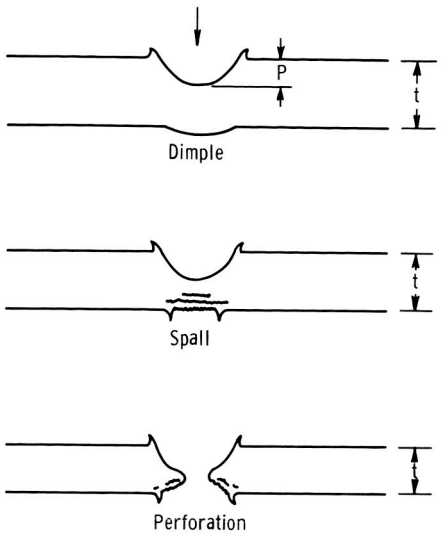

Figure 1. - Definition of damage modes.

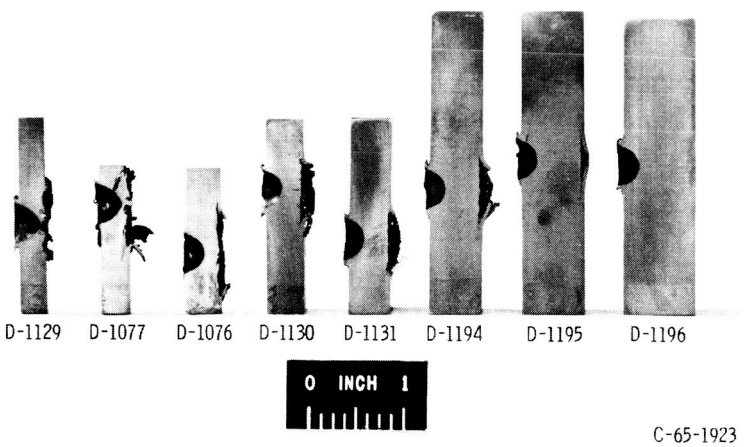

Figure 2. - Cratering, dimple, spall and perforation in columbium - 1-percent zirconium plates after impact of 1/8-inch pyrex projectile at 25,000 feet per second.

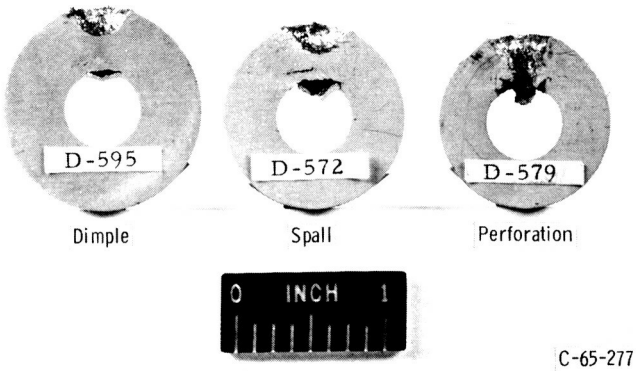

Figure 3. - Dimple, spall, and perforation in 1/2-inch-inside-diameter 2024-T6 aluminum tubes after impact of 3/32-inch pyrex projectiles at 25,000 feet per second.

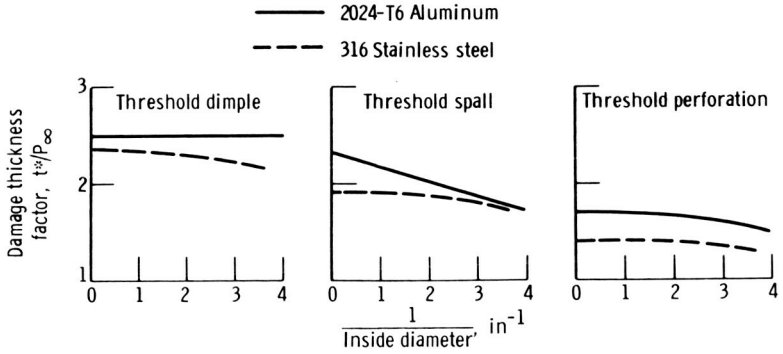

Figure 4. - Threshold dimple, spall, and perforation in unlined tubes of 316 stainless steel and 2024-T6 aluminum impacted by 3/32-inch pyrex projectile at 25,000 feet per second.

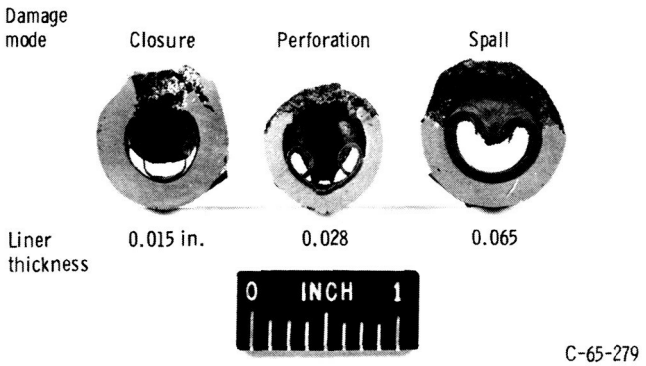

Figure 5. - Limiting damage modes in lined 316 stainless steel tubes armored with cast aluminum after impact at room temperature by 3/32-inch pyrex projectiles at 25,000 feet per second.

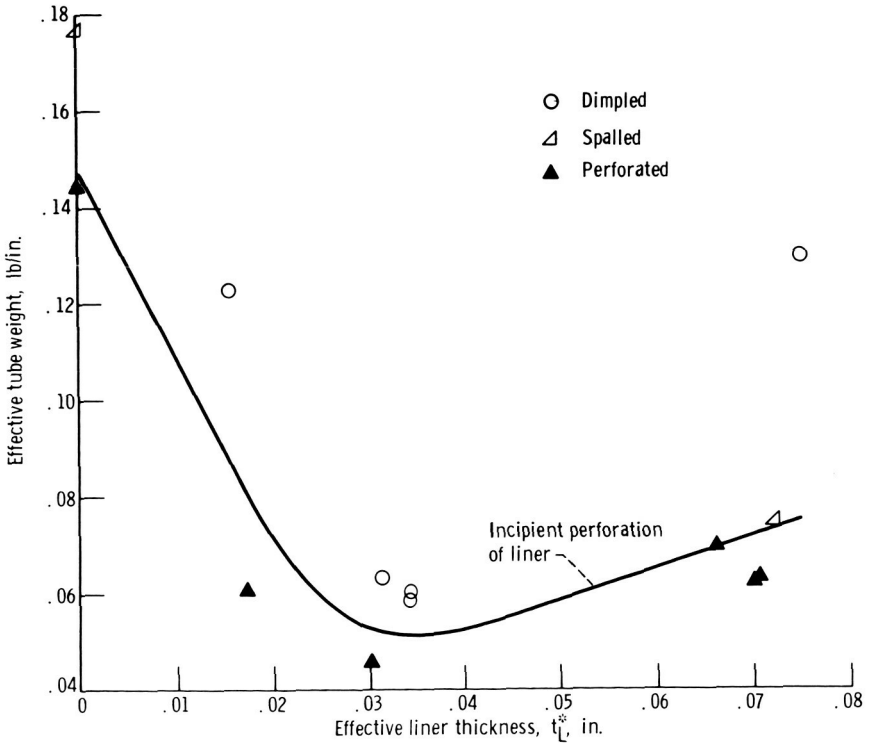

Figure 6. - Total effective tube weight per linear inch against effective liner thickness for 1/2-inch inside diameter tubes. Cast aluminum armor over 316 stainless steel liners. 3/32-inch pyrex projectile, 25,000 feet per second, room temperature.

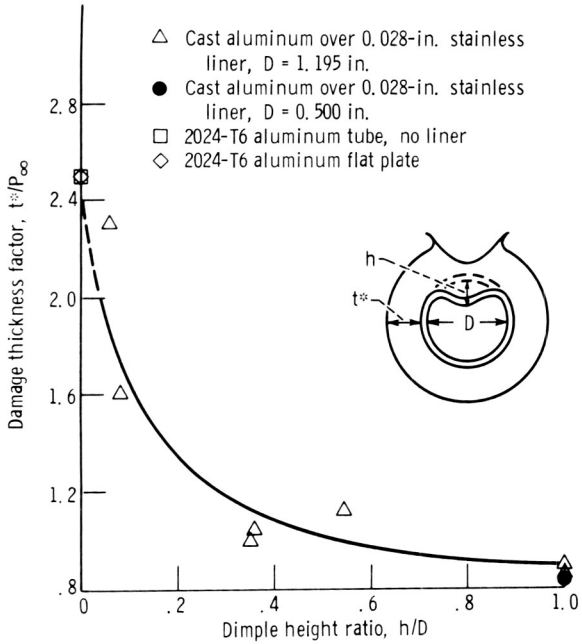

Figure 7. - Variation of damage thickness factor with dimple height, cast aluminum armor over 0.028-inch stainless steel liners. 3/32-inch pyrex projectiles, 25,000 feet per second, room temperature.

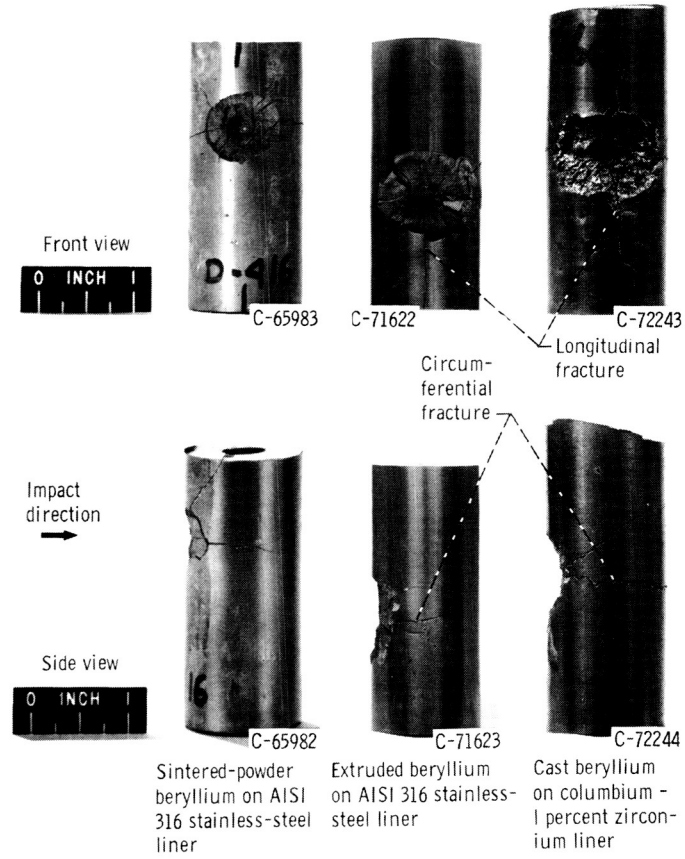

Figure 8. - Results of impact into beryllium - armored tubes fabricated by different processing methods. Impact velocity, 25 000 feet per second (nominal) with 3/32-inch-diameter pyrex sphere; target temperature, 1300° F.

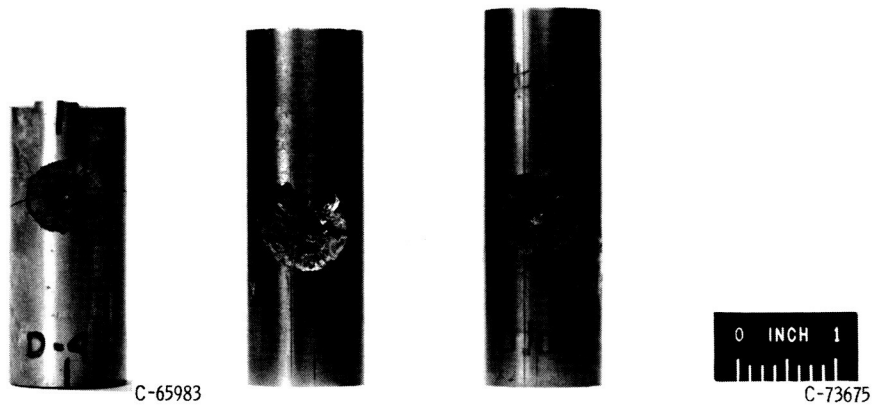

No reinforcement Fiber reinforcement Mesh reinforcement

Figure 9. - Results of impact into AISI 316 stainless steel reinforced beryllium armored tubes. Nominal impact velocity, 24,000 feet per second; 3/32-inch-diameter glass sphere; target temperature, 1300° F.

No internal reinforcement

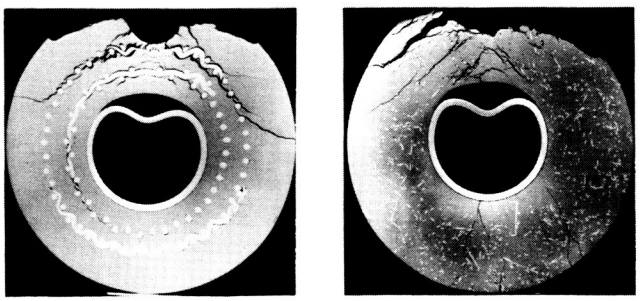

AISI 316 Stainless steel mesh reinforcement

AISI 316 Stainless steel fiber reinforcement

Figure 10. - Polished cross sections of internally reinforced and plain sintered powder beryllium armored AISI 316 stainless steel tubes after impact. Nominal impact velocity, 24,000 feet per second; 3/32-inch-diameter glass sphere target; temperature, 1300° F.

Material	γ	a
Columbium - 1-percent zirconium	1.49	4.50
Nickel (Inconel 718)	1.73	3.00
Cobalt (L-605)	1.81	2.50
Stainless steel (316)	1.90	2.40
Molybdenum (TZM)	1.90	2.50*
Vanadium	1.68	2.50*
Graphite (ATJ)	1.14	1.75
Beryllium	2.28	1.75

*Estimated value

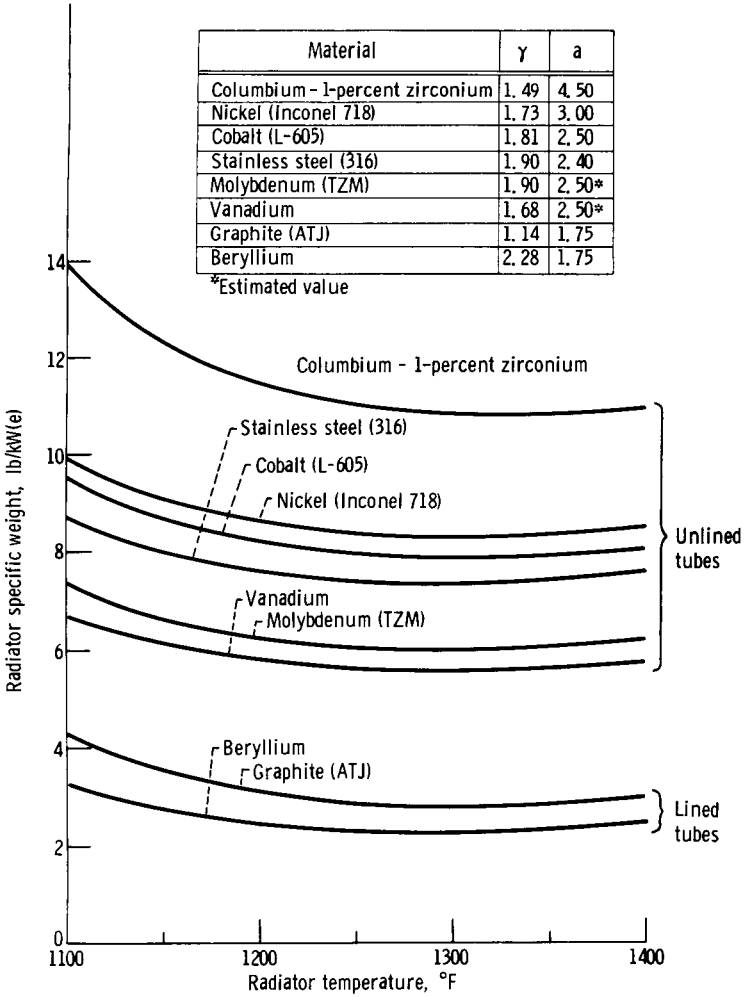

Figure 11. - Radiator specific weights for various armor materials using experimental materials coefficients γ and damage thickness factors a. No spall allowed.

Material	γ	Damage factors	
		Prevent spall	Prevent perforation
Columbium - 1-percent zirconium	1.49	4.50	2.10
316 Stainless steel	1.90	2.40	1.90

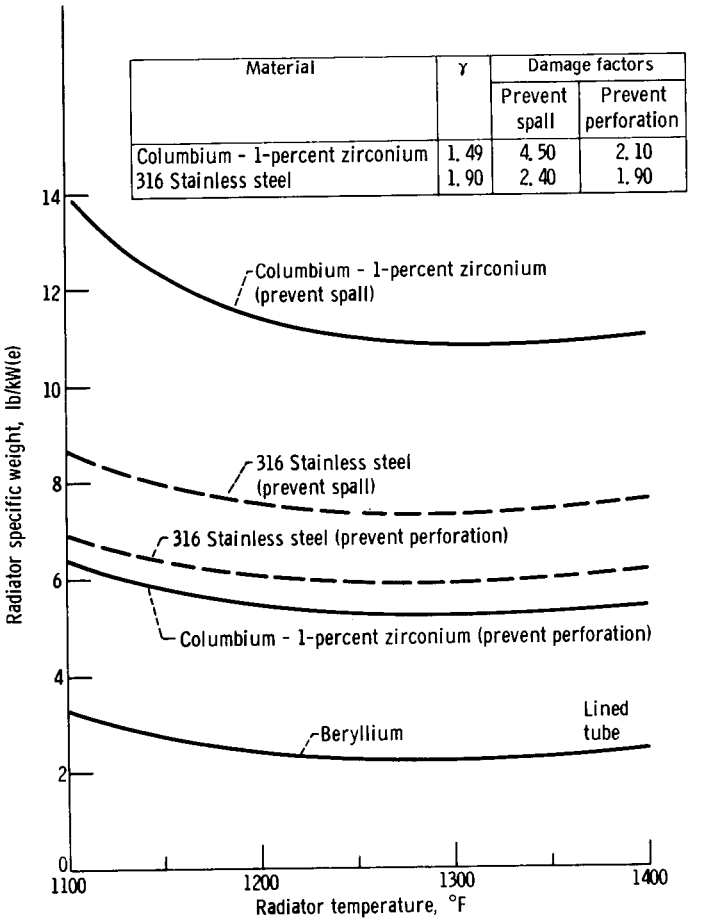

Figure 12. - Effect of designing for prevention of perforation or spall on radiator specific weights for columbium alloy and 316 stainless steel armor.

NASA-CLEVELAND, OHIO E-3215